

Fig. 1).

Molecules containing more than one ground state atom can be described with the same formalism. Two ground state atoms inside the electron orbit essentially do not interact with each other, since the Rb atom-atom scattering length [20] is much smaller than the mean particle distance in a dilute thermal cloud. Hence, the binding energy of an i -atomic molecule, $i \in \mathbb{N}$, is $(i - 1)$ times larger than the binding energy of a dimer. Only when the number of ground state atoms inside the Rydberg atom becomes very large, a change in the description of the system from discrete bound states to a mean field approximation is required (Fig. 1). In this case no individual bound states are resolved, but the Rydberg line is shifted by

$$\begin{aligned} \Delta E &= \iint d\mathbf{r} d\mathbf{R} V_{\text{pseudo}}(\mathbf{r}, \mathbf{R}) |\Psi(\mathbf{r})|^2 \rho(\mathbf{R}) \\ &= \int d\mathbf{R} V(\mathbf{R}) \rho(\mathbf{R}) = \frac{2\pi\hbar^2 a}{m_e} \bar{\rho}. \end{aligned} \quad (3)$$

If higher order corrections to the zero-energy scattering length can be neglected, the mean shift depends only on the value of a and the density $\bar{\rho}$ averaged over the volume of the Rydberg atom.

We perform the experiment in a magnetically trapped ultracold cloud of ^{87}Rb atoms in the $5S_{1/2}$, $F=2$, $m_F=2$ ground state with typical temperatures of $2 \mu\text{K}$ and densities on the order of 10^{12} cm^{-3} . Detailed information about the setup can be found in [21]. After the preparation of the ultracold cloud we excite the atoms in a two photon process via the $6P_{3/2}$ state to the $nS_{1/2}$ Rydberg state. For our high precision spectroscopy measurements we use narrow bandwidth lasers ($\leq 30 \text{ kHz}$), which are locked to a high finesse ULE reference cavity. The 420 nm light, driving the lower transition, is blue detuned from the intermediate state by 80 MHz to avoid absorption and heating of the cloud. It is sent to the experiment in $50 \mu\text{s}$ pulses with a repetition rate of 167 Hz. During the sequence the 1016 nm laser light driving the upper transition is on constantly. After the excitation we field-ionize the Rydberg atoms and collect the ions on a microchannel plate detector. In a single atomic cloud we perform typically 400 cycles of Rydberg excitation and detection while scanning the frequency of the blue laser light. In order to realize high spectral resolution we choose long excitation pulses of $50 \mu\text{s}$. Taking further into account the laser bandwidth, Doppler broadening and natural linewidth this results in an experimental resolution of around 60 kHz. In order to obtain the best visibility while changing the principal quantum number of the excited Rydberg state, we adjust the power of the blue laser to account for power broadening. Only the spectrum of $n=51$ was taken with higher laser power and thus in this case the atomic line is slightly broadened.

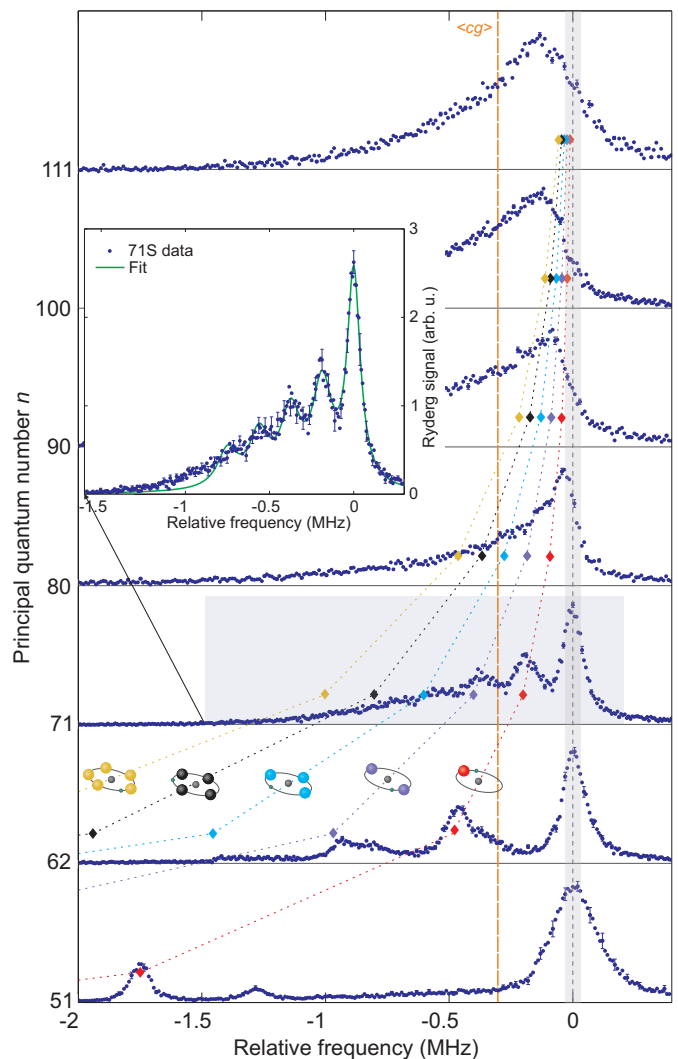


FIG. 2: Overview of the $5S_{1/2}$ to $nS_{1/2}$ excitation spectra showing the dimer - polymer transition for increasing principal quantum number. The origin of the relative frequency axis corresponds to the center of the atomic line (dashed line) for $n \leq 71$, where molecular lines are distinguishable. The gray shaded area between -30 kHz and 30 kHz indicates the laser bandwidth. Spectra at $n > 71$ are horizontally shifted such that their centers of gravity overlap with the mean center of gravity $\langle cg \rangle$ (orange dashed line) of the first three spectra ($n=51, 62, 71$). All data was taken at similar cloud parameters, therefore the density induced shift for all spectra is constant to first approximation. Molecules with up to three bound ground state atoms for $62S$ and up to four for $71S$ are resolvable in the spectra. Colored diamonds indicate the positions of the dimers (red), trimers (violet) etc. following the power law scaling of the binding energies fitted to the first three spectra. In the inset the molecular spectrum for the $n=71$ Rydberg state is shown. A multilorentzian fit (green line), assuming a constant spacing between the molecular peaks is plotted to indicate the positions of the higher order molecular lines. The spectrum for $n=40$ is not shown, because the binding energy of the dimer is larger than the plotting range. Each spectrum is an average over 20 independent measurements with standard deviation error bars.

In Fig. 2 excitation spectra from the $5S_{1/2}$ to the $nS_{1/2}$ state, where n is ranging from 51 to 111, are presented. The shape of the obtained Rydberg spectra varies significantly for different n . For low principal quantum numbers clearly distinguishable molecular lines are present on the red side of the atomic peak, which is situated at the origin. In the spectrum of $n=51$ the peak at -1.7 MHz can be identified as a dimer, for which the ground state atom is localized in the outermost well of the molecular potential. Additionally at -1.3 MHz an excited vibrational state [8, 19] is visible. For a given density, the probability to find an atom inside the electron orbit scales as n^{*6} with the effective principal quantum number $n^* = n - \delta$, where δ is the quantum defect. Hence, higher order molecules are formed more likely at higher n . At the same time the binding energy per atom decreases and thus polyatomic molecular lines become visible in the spectra of $n=62$ and 71. The binding energy E_B can be directly measured as the difference between the atomic and the molecular line in the spectrum. At $n=62$ lines up to the tetramer together with corresponding vibrational excited states are visible. The broadening of the tetramer line may be caused by the presence of these excited states, possibly with a reduced lifetime [22]. At $n=71$ only vibrational ground states are resolved. Polyatomic molecules up to a pentamer can be identified. The size of such a molecule becomes enormous due to the Rydberg electron orbit radius reaching almost $10\,000a_0$. For large n the binding energy E_B decreases until it is below the experimental resolution. This manifests in a non-resolvable shoulder and finally in an inhomogeneously broadened spectral line.

The experimental binding energies can be calculated based on the molecular potential (2) and the mean shift (3). We use corrections to the s -wave scattering length including terms linear in the relative momentum of two scattering partners based on a semiclassical approximation [17]. This approximation is valid for large distances from the ionic core. Therefore we restrict the analysis only to the lowest bound state. The discussion of higher vibrational states can be found in [19]. We solve the Schrödinger equation for the ground state atom in the molecular potential using Numerov's method and fit the zero-energy scattering length a to the binding energies of the dimers. In this paper the best agreement with the experimental data is obtained for $-16.2a_0$, which is very close to the theoretically predicted value of $-16.1a_0$ [16].

For $n > 71$, where no distinct molecular lines can be identified, a mean field description is required. Furthermore, the spectral position of pure Rydberg atoms, and thus the zero position, cannot be identified directly from the signal. However it can be determined from the center of gravity cg of the spectra, taken in a non-blockaded sample, which is constant for a given density. Intuitively, this result in the first approximation can be ex-

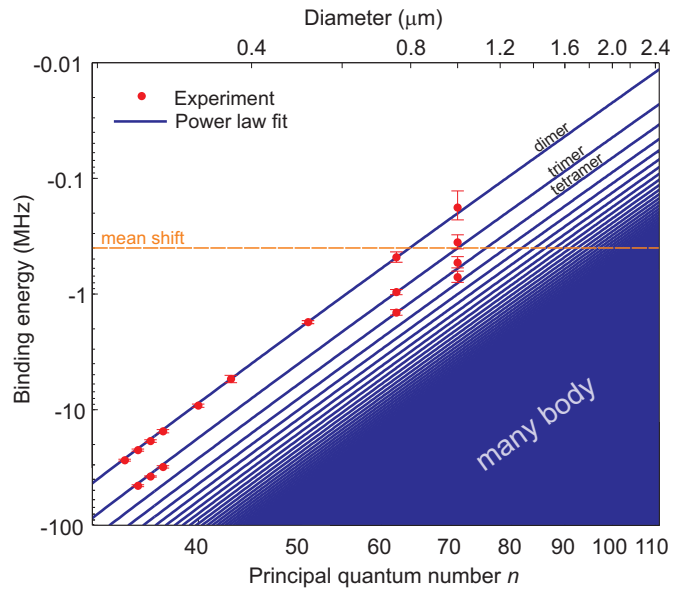


FIG. 3: Measured binding energies (red points) versus principal quantum number (bottom axis) and diameters (top axis) of the molecules. The data for $n \leq 37$ is taken from [8]. For $n=40, 43, 51$ the frequency range chosen in the experiment was too small to photoassociate molecules with larger binding energies than a dimer. The power law n^{*b} (blue lines) fitted to the measured data and multiplied by factors $i-1$, $i \in \mathbb{N}$, ($i=2$ for a dimer) shows that for $n > 75$ the binding energy of the dimer becomes smaller than the experimental resolution. The increasing number of ground state atoms inside the electron orbit leads eventually to a mean shift of the Rydberg line. Calculated values of E_B are not shown in the plot, because they are hardly distinguishable from the experimental data on this scale. The error bars are determined as the standard deviation of the fit.

plained by the fact, that while the mean potential depth $\bar{V} = \frac{\int d\mathbf{R} V(\mathbf{R})}{\int d\mathbf{R}}$ averaged over the volume of the Rydberg atom decreases with the effective principal number as n^{*-6} , the probability to find an atom inside the Rydberg electron orbit increases with n^{*6} . In the experiment all data was taken at a fixed density. Thus, in our analysis we overlap the center of gravity of the spectra at $n \geq 71$ with the mean $\langle cg \rangle = -300$ kHz determined at low principal quantum numbers. Doing so we can identify the zero position in the top panels of Fig. 2. Assuming the scattering length a to be constant, we determine the effective density to be $3 \cdot 10^{12} \text{ cm}^{-3}$, which is close to the peak density obtained from a Gaussian fit to absorption images of the thermal cloud. This indicates that molecules are most likely created in regions of high density. Only for $n \leq 80$ the highest signal originates from pure Rydberg atoms. Already for $n=80$ there is on average one ground state atom inside the electron orbit, leading to a high probability to excite dimers instead of pure Rydberg atoms. On average there are four atoms inside the 100S electron orbit and eight for the 111S state. Therefore,

the atomic line is suppressed, while the molecular lines are not resolvable in the experiment any more, caused by their very low binding energies. According to the central limit theorem, for even higher principal quantum numbers the shape of the spectrum is expected to become Gaussian, with the maximum at the position of the mean shift ($\langle cg \rangle$ in Fig. 2). The density dependent dephasing resulting from the existence of many molecular lines within the Rydberg line envelope sets a fundamental limit for the number of atoms inside the blockade radius i. e. the optical thickness. This fact is of importance for every experiment taken at high principal quantum numbers and high densities, in particular for quantum optics experiments in ultracold clouds [23–25].

The binding energies of all observed molecules are plotted in Fig. 3. From the extrapolated molecular binding energies the transition from the few particle description of discrete bound states to a mean field shift becomes visible. A power law fitted to the $n \geq 40$ data shows a scaling with the effective principal quantum number n^* to the power of -6.26 ± 0.12 , close to the value of -6 , expected from the size scaling argument. The deviation can be explained by the dependence of the scattering length on the relative momentum and the fact, that with increasing principal quantum number the shape of the outermost well of the molecular potential changes. Taking the corresponding zero-point energy and momentum dependent corrections to the scattering length into account, we obtain an exponent of -6.37 , which is in very good agreement with our experimental data. Contributions of higher order partial waves and p -wave shape resonances to the molecular potential can be neglected since the kinetic energy associated with the relative motion of two scattering partners is small in the region of interest.

Rydberg molecules in an ultracold cloud constitute a tunable model system to study the transition from a few-body to a many-body regime. They offer a unique tool to address few-body subsystems with control on a single particle level by changing the detuning of the excitation laser light. Complementary to this work the number of constituents and the interaction strength can be also varied independently by changing the density and the principal quantum number of the excited Rydberg atom. Furthermore, the analysis of the relative strength of the molecular lines opens up the possibility to measure correlations in a bosonic gas. In high density gases and for low principal quantum numbers, where the size of the Rydberg atom is comparable to the de Broglie wavelength, extracting the $g^{(2)}$ correlation function [26] of thermal and Bose-condensed gases is feasible. In addition to previous measurements [27, 28] also higher order correlation functions can be studied using polyatomic molecules.

We acknowledge support from Deutsche Forschungsgemeinschaft (DFG) within the SFB/TRR21 and the project PF 381/4-2. Parts of this work was also founded by ERC under contract number 267100. A.G. acknowl-

edges support from E.U. Marie Curie program ITN-Coherence 265031 and S.H. from DFG through the project HO 4787/1-1.

The experiment was conceived by A.G., A.T.K., R.L., S.H. and T.P. and carried out by A.G. and A.T.K.; data analysis was accomplished A.G. and A.T.K.; numerical calculation is by A.G. and J.B.B. and A.G. wrote the manuscript with contributions from all authors.

The authors declare that they have no competing financial interests.

* Electronic address: a.gaj@physik.uni-stuttgart.de

† Electronic address: t.pfau@physik.uni-stuttgart.de

- [1] Hartman, M., Miller, R. E., Toennies, J. P. & Vilesov, A. F. High-resolution molecular spectroscopy of van der Waals clusters in liquid helium droplets. *Science* **272**, 1631–1634 (1996).
- [2] Wenz, A. *et al.* From few to many: Observing the formation of a Fermi sea one atom at a time. *Science* **342**, 457–460 (2013).
- [3] Greene, C. H., Dickinson, A. S. & Sadeghpour, H. R. Creation of polar and nonpolar ultra-long-range Rydberg molecules. *Phys. Rev. Lett.* **85**, 2458–2461 (2000).
- [4] Herbig, J. *et al.* Preparation of a pure molecular quantum gas. *Science* **301**, 1510–1513 (2003).
- [5] Köhler, T., Góral, K. & Julienne, P. S. Production of cold molecules via magnetically tunable Feshbach resonances. *Rev. Mod. Phys.* **78** (2006).
- [6] Butscher, B. *et al.* Atom-molecule coherence for ultralong-range Rydberg dimers. *Nature Phys* **6**, 1745–2473 (2010).
- [7] Li, W. *et al.* A homonuclear molecule with a permanent electric dipole moment. *Science* **334**, 1110–1114 (2011).
- [8] Bendkowsky, V. *et al.* Observation of ultralong-range Rydberg molecules. *Nature* **458**, 0028–0836 (2009).
- [9] Krupp, A. T. *et al.* Alignment of D-state Rydberg molecules. *Phys. Rev. Lett.* **112**, 143008 (2014).
- [10] Anderson, D. A., Miller, S. A. & Raithel, G. Photoassociation of long range nd Rydberg molecules. *arXiv:1401.2477* (2014).
- [11] Bellos, M. A. *et al.* Excitation of weakly bound molecules to trilobitelike Rydberg states. *Phys. Rev. Lett.* **111**, 053001 (2013).
- [12] Tallant, J., Rittenhouse, S. T., Booth, D., Sadeghpour, H. R. & Shaffer, J. P. Observation of blueshifted ultralong-range Cs₂ Rydberg molecules. *Phys. Rev. Lett.* **109**, 173202 (2012).
- [13] Balewski, J. B. *et al.* Coupling a single electron to a Bose-Einstein condensate. *Nature* **502**, 664–667 (2013).
- [14] Amaldi, E. & Segrè, E. Effect of pressure on high terms of alkaline spectra. *Nature* **133**, 141 (1934).
- [15] Fermi, E. Sopra lo spostamento per pressione delle righe elevate delle serie spettrali. *Nuovo Cimento* **11**, 157–166 (1934).
- [16] Bahrim, C., Thumm, U. & Fabrikant, I. I. ³Se and ¹Se scattering lengths for $e^- + \text{Rb, Cs and Fr}$ collisions. *J. Phys. B: At. Mol. Opt. Phys.* **34**, L195–L201 (2001).
- [17] Omont, A. On the theory of collisions of atoms in Rydberg states with neutral particles. *J. Phys. France* **38**,

- 1343–1359 (1977).
- [18] Hamilton, E. L., Greene, C. H. & Sadeghpour, H. R. Shape-resonance-induced long-range molecular Rydberg states. *J. Phys. B: At. Mol. Opt. Phys.* **35** (2002).
- [19] Bendkowsky, V. *et al.* Rydberg trimers and excited dimers bound by internal quantum reflection. *Phys. Rev. Lett.* **105**, 163201 (2010).
- [20] Julienne, P. S., Mies, F. H., Tiesinga, E. & Williams, C. J. Collisional stability of double Bose condensates. *Phys. Rev. Lett.* **78**, 1880 (1997).
- [21] Löw, R. *et al.* An experimental and theoretical guide to strongly interacting Rydberg gases. *J. Phys. B: At. Mol. Opt. Phys.* **45**, 113001 (2012).
- [22] Butscher, B. *et al.* Lifetimes of ultralong-range Rydberg molecules in vibrational ground and excited states. *J. Phys. B: At. Mol. Opt. Phys.* **44**, 184004 (2011).
- [23] Peyronel, T. *et al.* Quantum nonlinear optics with single photons enabled by strongly interacting atoms. *Nature* **488**, 57–60 (2012).
- [24] Dudin, Y. O., Li, L., Bariani, F. & Kuzmich, A. Observation of coherent many-body Rabi oscillations. *Nature Phys* **8** (2012).
- [25] Baur, S., Tiarks, D., Rempe, G. & Dürr, S. Single-photon switch based on Rydberg blockade. *Phys. Rev. Lett.* **112**, 073901 (2014).
- [26] Naraschewski, M. & Glauber, R. J. Spatial coherence and density correlations of trapped Bose gases. *Phys. Rev. A* **59**, 6 (1999).
- [27] Burt, E. A. *et al.* Coherence, correlations, and collisions: What one learns about Bose-Einstein condensates from their decay. *Phys. Rev. Lett.* **79** (1997).
- [28] Hodgman, S. S., Dall, R. G., Manning, A. G., Baldwin, K. G. H. & Truscott, A. G. Direct measurement of long-range third-order coherence in Bose-Einstein condensates. *Science* **331**, 1046–1049 (2011).